The International Journal of Advanced Manufacturing Technology (2023) 126:1379–1395
https://doi.org/10.1007/s00170-023-11181-y

ORIGINAL ARTICLE

A geometric error measurement method for five-axis ultra-precision machine tools

Luqi Song[1] · Xueshen Zhao[1] · Qiang Zhang[1] · Dequan Shi[1] · Tao Sun[1]

Received: 17 August 2022 / Accepted: 26 February 2023 / Published online: 10 March 2023
© The Author(s), under exclusive licence to Springer-Verlag London Ltd., part of Springer Nature 2023

Abstract
To solve the problem of geometric error measurement for five-axis ultra-precision machine tools in interpolated five-axis motion, a measurement method based on the double ballbar (DBB) is proposed in this paper. The method proposed in this research can measure the geometric errors of five-axis ultra-precision machine tool through only one-time installation, and the new method is less limited by the layout of machine tools. The motion trajectory is designed, and the length of the DBB remains constant during the measurement process to achieve the measurement of the geometric errors. Furthermore, the measured results are compared with the theoretical results of the error model. It is found that the trend and the amplitude of the measurement results are in agreement with the theoretical results. It is proved that the method can measure the geometric errors of five-axis ultra-precision machine tool effectively.

Keywords Ultra-precision machine tool · Double ballbar · Five-axis · Geometric error

1 Introduction

With the development of technology, the demand for the ultra-precision machining of parts with complex shapes is increasing, and the increase in the number of machine tool axes has become a development trend for ultra-precision machine tools. As the number of machine tool axes increases, the geometric error terms of machine tools also increase. A three-axis ultra-precision machine tool contains 24 geometric error terms, while a five-axis ultra-precision machine tool contains 43 geometric error terms [1, 2]. During the machining process, the error terms of the axis are coupled with other error terms, causing the tool to deviate from the perfect functional point and finally forming the machining error of the machine tool. If researchers want to improve the machining accuracy of machine tools, it is necessary to compensate for errors [3], but the premise of error compensation is to measure errors accurately, so it is very important to study the error measurement of ultra-precision machine tools.

In ultra-precision machine tools, the geometric error is an important factor affecting the machining accuracy of parts [4]. However, due to the characteristics of small batches and the strong customization of ultra-precision machine tools, there is currently no mature testing standard. The methods in the standards ISO-230–1 to ISO-230–7 are mainly used to detect the geometric errors of ultra-precision machine tools [5]. In previous studies, scholars have performed a large amount of work on the detection and identification of machine tool geometric errors, and many results have been achieved.

For the linear axis, a laser interferometer was generally used to measure the positioning error and straightness error [6]. In addition, some scholars proposed various identification methods for the geometric errors of linear axes based on laser trackers [7], photoelectric autocollimators [8], and other instruments. The geometric error of the rotary axis includes the radial error and the axial error, which can be measured using the *R*-test [1, 9]. Ibaraki [10], Jiang [11], and Chen [12] installed a trigger probe or stylus on machine tools and used the on-machine measurement method to measure the geometry error of the rotary axis on a five-axis ultra-precision machine tool. Other scholars used instruments such as double ballbar (DBB) [13], laser displacement sensor, and interference sensor of angular micro deflection [14] to measure the geometric error of the rotary axis. There is also

✉ Tao Sun
taosun@hit.edu.cn

[1] Center for Precision Engineering, Harbin Institute of Technology, Harbin, China

a squareness error between the axes in machine tools. The squareness error can be measured with displacement sensors and a standard square ruler [15], and it can be quickly measured using a DBB [6].

Except for the above errors, in some cases, the diagonal error of machine tools will also be a matter of concern. By measuring the diagonal error, the squareness error and geometric error terms can be indirectly evaluated [16]. The body diagonal error can be measured using a laser interferometer [5]. Wang firstly presented the step-diagonal test [5], and then, Chapman[17] and Ibaraki [18] studied the issues in the step-diagonal test. Sun et al. [19] developed a method for measuring the body diagonal error with a multi-beam laser interferometer and measured the body diagonal error of a five-axis machining center. Yang et al. [20] measured the face diagonal error and body diagonal error with a DBB.

In addition, some scholars developed different measuring instruments and methods to measure the geometric errors of machine tools. Kim et al. [21] proposed that if quantum entangled states were preset in photons, the measurement accuracy of an interferometer could be improved by 100 times under the same conditions. Hong et al. [22] used a non-contact laser displacement sensor to replace the contact displacement sensor in a traditional *R*-test instrument and measured the rotary axis error of a machine tool. Wang et al. [23] developed a new measuring instrument J-DBB that added a ball joint structure to a traditional DBB and effectively improved the measurement space.

The methods described above all directly measured the machine tool's geometric error, and they could also indirectly evaluate the geometric error of the machine tool by measuring the error of the test part. Currently, the commonly used test parts include the NAS 979 test part [24], the M1 to M4 test parts proposed in ISO 10791–7:2020 [25], and the S-shaped test part [26]. Ibaraki [27–29] analyzed the geometric error of a five-axis machining center, designed and processed a variety of different forms of test parts, and verified the machine tool error in reverse. Liu [4] and Gao [6] et al. obtained the geometric error for a three-axis ultra-precision machine tool according to the test part error.

Although scholars have proposed many measurement methods for geometric errors, most of them are aimed at the geometric errors of a single axis or some error terms. When all five axes of the machine tool are required to participate in the machining, due to the couple relationship of all the errors, it is difficult to identify and measure the geometric errors. It requires repetitive and tedious work to measure all the error terms of a five-axis ultra-precision machine tool with many specialized instruments, and the measurement results need to be simulated based on the error model to obtain the geometric error curves in interpolated five-axis motion. Many scholars [6, 13, 20, 23] used DBB to measure different geometric errors. Ni [13], Chu [30], Wang [31], Chen [32], and other scholars obtained the rotary axis geometric errors by designing the motion trajectory of machine tools to ensure that the length of the DBB keeps constant during the measurement process. A measurement method of five-axis machine tool geometric errors is mentioned in ISO 230–1 [2]; in order to exercise all axes of motion, the workpiece rotary axis needs to rotate to a certain angle. However, this method can only be used on machine tools with two serial rotary axes, and thus, the method is limited by the machine tool layout.

As a five-axes motion trajectory is designed, the length of the DBB is kept constant to measure the geometric error of the machine tool in the interpolated five-axis motion. The geometric error measurement results can provide guidance for the design and error compensation of machine tools, reduce the error of machine tools, and improve machining accuracy.

In this research, a measurement method is proposed for the geometric error measurement problem of five-axis ultra-precision machine tools in interpolated five-axis motion. The principle of the measurement method and the method of instrument installation and adjustment are described in Sect. 2. The error measurement experiment is carried out on a five-axis ultra-precision machine tool in Sect. 3. Finally, the measurement results and the theoretical calculation results are compared and discussed in Sect. 4.

2 Methodology

2.1 Motion trajectory design

The DBB is a high-precision linear telescopic sensor, the two ends of which are connected with a precision sphere. The measurement of the distance change between the two spheres can reflect the errors of machine tools, such as the squareness error and backlash, which have been included in ISO 230–1:2012 [2].

The five-axis ultra-precision machine tool studied in this research is illustrated in Fig. 1. The machine tool contains five axes, including the three linear axes of *X*, *Y*, and *Z*, and the two rotary axes of *B* and *C*, adopting the *w*–*C*-*Y*–*Z*-*b*-*X*-*B*-*t* layout, where *w* means workpiece, *b* means machine bed, and *t* means tool. The *X*-axis and the *Z*-axis are vertically set on the base. The *Y*-axis is set on the *Z*-axis, which can drive the *C*-axis to move in the *Y* direction. The *B*-axis is set on the *X*-axis.

When the two spheres of the DBB are installed on the *B*-axis and *C*-axis of the machine tool, respectively, the motion trajectory of the five axes can be designed accordingly. The positions of the two spheres change steadily according to the designed test trajectory. The designed test trajectory must ensure that the distance between the two

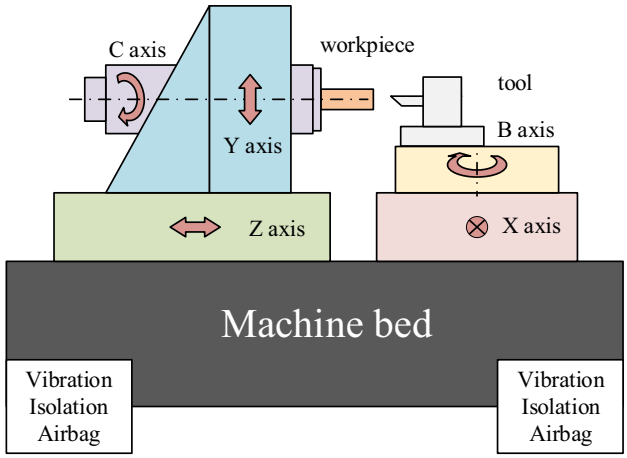

Fig. 1 Five-axis ultra-precision machine tool structure

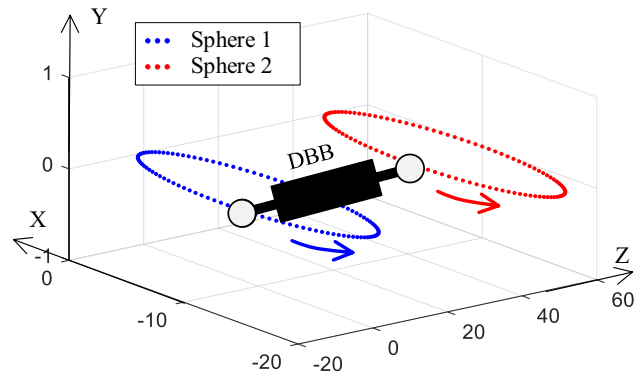

Fig. 2 DBB sphere movement tracks

spheres of the DBB remains constant, and the direction of the DBB is parallel to the tested axis. However, because of the manufacturing, assembly, and control errors of the machine tool, the relative position of the two spheres will change inevitably, and thus, the geometric error of the machine tool in interpolated five-axis motion can be measured by the DBB. Therefore, the principle of the motion trajectory design is that the relative position of the two spheres of the DBB remains constant.

It is assumed that the sphere attached on the C-axis is sphere 1, and the sphere attached on the B-axis is sphere 2. When sphere 1 rotates with the C-axis, its X and Y coordinates also change accordingly. Assuming that the rotation angular velocity of the C-axis is ω_1, the distance between sphere 1 and the C-axis rotation axis is R_1, and the initial angle is the positive direction of the Y-axis, and the position of sphere 1 at time t can be described as

$$\begin{cases} x_1(t) = -R_1 sin(\omega_1 t) \\ y_1(t) = -R_1\left[1 - \cos(\omega_1 t)\right] \end{cases} \tag{1}$$

where x_1 (t) and y_1 (t) are the X and Y coordinates of the center of sphere 1, respectively.

In the same way, assuming that the rotational angular velocity of the B-axis is ω_2, the distance between sphere 2 and the B-axis rotation axis is R_2, and the initial angle is the positive direction of the Z-axis, and the position of sphere 2 at time t can be described as

$$\begin{cases} x_2(t) = R_2 sin(\omega_2 t) \\ z_2(t) = -R_2\left[1 - \cos(\omega_2 t)\right] \end{cases} \tag{2}$$

where x_2 (t) and z_2 (t) are the X and Z coordinates of the center of sphere 2, respectively.

First, it is assumed that $\omega_1 = \omega_2$ to synchronize the motion of the two spheres. When the C-axis rotates, the X-axis moves as x_1 (t) to compensate for the displacement of sphere 1 in the X direction, and the Y-axis moves as $-y_1$ (t) to compensate for the displacement of sphere 1 in the Y direction. When the B-axis rotates, the X-axis moves as $-x_2$ (t), and the Z-axis moves as z_2 (t) to compensate for the displacement of sphere 2 in the X direction and the Z direction. It is evident that when the B-axis and the C-axis rotate at the same angular velocity ω, the X-axis moves as x_1 $(t) - x_2$ (t), the Y-axis moves as $-y_1$ (t), and the Z-axis moves as z_2 (t), the relative position of the two spheres remains synchronized. The final designed motion trajectory can be described as

$$\begin{cases} \theta_B(t) = \omega t \\ \theta_C(t) = \omega t \\ x(t) = -\left(R_1 + R_2\right) sin(\omega t) \\ y(t) = R_1[1 - \cos(\omega t)] \\ z(t) = -R_2[1 - \cos(\omega t)] \end{cases} \tag{3}$$

where θ_B (t) and θ_C (t) are the B-axis and C-axis motion trajectories, respectively, and x (t), y (t), and z (t) are the X-axis, Y-axis, and Z-axis motion trajectories, respectively.

Assuming that $R_1 = R_2 = 10$ mm, the length of the DBB is 50 mm. According to Eq. (3), the motion trajectory of the two spheres when the DBB is installed toward the Z direction can be drawn as demonstrated in Fig. 2.

The positions of the two spheres are solved separately, and the change of the coordinates of sphere 1 with time is deduced as

$$\begin{cases} x_1'(t) = x_1(t) = -R_1 \cdot sin(\omega t) \\ y_1'(t) = y_1(t) + y(t) = -R_1[1 - \cos(\omega t)] + R_1[1 - \cos(\omega t)] = 0 \\ z_1'(t) = z(t) = -R_2 \cdot (1 - \cos\omega t) \end{cases} \tag{4}$$

The change of the coordinates of sphere 2 with time is deduced as

$$\begin{cases} x_2'(t) = x_2(t) + x(t) = R_2 sin(\omega t) - \left(R_1 + R_2\right) sin(\omega t) = -R_1 sin(\omega t) \\ y_2'(t) = 0 \\ z_2'(t) = z_2(t) = -R_2[1 - \cos(\omega t)] \end{cases} \tag{5}$$

Subtracting Eq. (4) from Eq. (5) can produce the relative position relationship of the two spheres under ideal conditions, as shown below:

$$\begin{cases} \Delta x(t) = x_1'(t) - x_2'(t) = 0 \\ \Delta y(t) = y_1'(t) - y_2'(t) = 0 \\ \Delta z(t) = z_1'(t) - z_2'(t) = 0 \end{cases} \tag{6}$$

According to Eq. (6), when the machine tool moves with the motion trajectory set by Eq. (3), the two spheres of the DBB remain relatively static for the case of no error.

The DBB is installed toward the X, Y, and Z directions, as illustrated in Fig. 3, the error curves δ_x (t), δ_y (t), and δ_z (t) are measured, respectively. Since the starting positions of the X-, Y-, and Z-axes are different during the measurement process, the peak-valley (PV) values δ_x, δ_y, and δ_z of the error curves are taken as the error values in each direction. The total geometric error δ of the machine tool in interpolated five-axis motion can be described as

$$\delta = \sqrt{\delta_x^2 + \delta_y^2 + \delta_z^2} \tag{7}$$

When the DBB is installed toward the X direction, the errors in the Y and Z directions of the machine tool affect the measurement results. Similarly, when the DBB is installed toward the Y and Z directions, it is also affected by the errors in the other directions. With the assumption that the DBB is installed toward the X direction, the error in the Y direction can be taken as an example to calculate its influence on the measurement result. In the Y direction, there are mainly E_{YX} (straightness error of X-axis), E_{YY} (positioning error of Y-axis), E_{YZ} (straightness error of Z-axis), and other error terms. The Y direction error is usually in the order of 5–10 μm, and the length of the DBB is 50 mm. Assume that the error in Y direction is 10 μm, the influence Δ of the Y direction error on the length of the DBB can be calculated as

$$\Delta = \sqrt{50^2 + 0.01^2} - 50 = 1.6\text{E} - 6\text{mm} \tag{8}$$

Based on the above calculation results, the deformation of the length of the DBB caused by the error in the non-sensitive direction does not have an impact on the measurement results, so this method can accurately measure the error.

2.2 Installation errors analysis

According to Eq. (3), the motion trajectory of the five axes of the machine tool can be fully defined by ω, R_1, and R_2, while the ω is controlled by the numerical control (NC) program, and only the length of the R_1 and R_2 is needed to be measured accurately. At the same time, the B-axis and C-axis should rotate from the start angle 0°, so the orientations of R_1 and R_2 are also need to be measured accurately. Limited by the resolution of the measurement instrument, the lengths and orientations of R_1 and R_2 are not absolutely accurate. Therefore, it is necessary to measure and compensate the installation errors of the DBB. All the four installation errors are illustrated in Fig. 4.

If the installation errors of the DBB are measured with the five-axis NC program, three equations including the installation errors can be obtained, but the installation errors value is 4, which cannot be solved. Therefore, it is necessary to control the number of installation errors included in the equations so that the number of error equations is greater than or equal to the number of installation errors.

When the B-axis remains stationary and the C-axis rotates, there are only two installation errors (ΔR_1 and $\Delta\theta_1$) involved in the error curves. Likewise, when the C-axis remains stationary and the B-axis rotates, there are only two installation errors (ΔR_2 and $\Delta\theta_2$) involved in the error

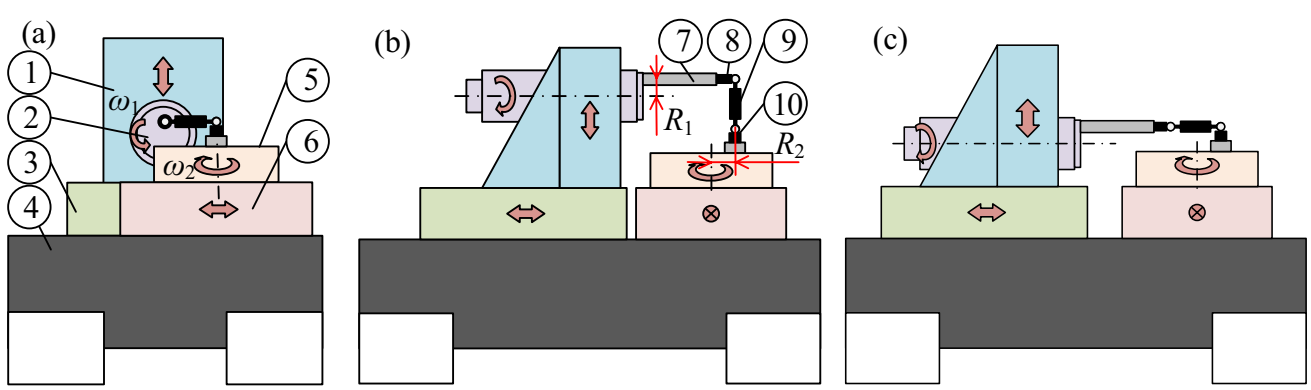

Fig. 3 Diagram of the DBB installation: **a** X direction, **b** Y direction, and **c** Z direction

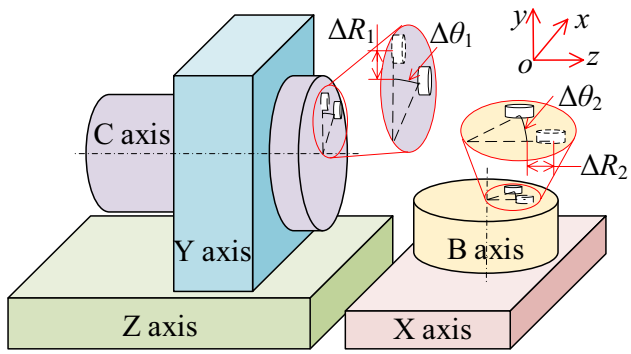

Fig. 4 Diagram of the DBB installation errors

curves. Therefore, by designing the motion trajectories of XYC and XZB and measuring the respective errors, four equations including the installation errors can be obtained.

The XYC motion trajectory can be expressed as

$$\begin{cases} \theta_C(t) = \omega t \\ \theta_B(t) = 0 \\ x(t) = -R_1 sin(\omega t) \\ y(t) = R_1[1 - \cos(\omega t)] \\ z(t) = 0 \end{cases} \tag{9}$$

The XZB motion trajectory can be expressed as

$$\begin{cases} \theta_B(t) = \omega t \\ \theta_C(t) = 0 \\ x(t) = -R_2 sin(\omega t) \\ y(t) = 0 \\ z(t) = -R_2[1 - \cos(\omega t)] \end{cases} \tag{10}$$

If there is no error, then when the machine tool moves as shown in Eq. (9), the two sphere motion trajectories are the same, and the position remains relatively static. If there are installation errors ΔR_1 and $\Delta\theta_1$, the coordinates of sphere 1 change with time, as follows:

$$\begin{cases} x_1(t) = -\left(R_1 + \Delta R_1\right) \cdot sin\left(\omega t + \Delta\theta_1\right) \\ y_1(t) = y(t) - \left(R_1 + \Delta R_1\right) \cdot \left[1 - \cos\left(\omega t + \Delta\theta_1\right)\right] \\ z_1(t) = z(t) = 0 \end{cases} \tag{11}$$

The coordinates of sphere 1 that change with time are

$$\begin{cases} x_2(t) = x(t) = -R_1 \cdot sin\omega t \\ y_2(t) = 0 \\ z_2(t) = 0 \end{cases} \tag{12}$$

Because both ΔR_1 and $\Delta\theta_1$ are extremely small quantities, therefore, by letting $\cos\Delta\theta_1 \approx 1$, $\sin\Delta\theta_1 \approx \Delta\theta_1$, subtracting Eq. (12) from Eq. (11), and ignoring the higher-order error terms in the equation, when there are installation errors, the relative position between the two spheres is

$$\begin{cases} \Delta x(t) \approx -R_1\Delta\theta_1 cos\omega t - \Delta R_1 sin\omega t \\ \Delta y(t) \approx -R_1\Delta\theta_1 sin\omega t + \Delta R_1 cos\omega t - \Delta R_1 \\ \Delta z(t) = 0 \end{cases} \tag{13}$$

Based on trigonometry, Eq. (13) can be simplified to

$$\begin{cases} \Delta x(t) = -A_1 cos(\omega t - \varphi_1) \\ \Delta y(t) = A_1 sin(\omega t - \varphi_1) - \Delta R_1 \\ \Delta z(t) = 0 \end{cases} \tag{14}$$

where $A_1 = \sqrt{(R_1\Delta\theta_1)^2 + \Delta R_1^2}$ and $\varphi_1 = \arctan\left(\frac{\Delta R_1}{R_1\Delta\theta_1}\right)$.

It is easy to determine that the influence of ΔR_1 and $\Delta\theta_1$ on the measurement results in the X and Y directions is a sinusoid with the frequency $f = \omega/2\pi$. Therefore, with the sinusoidal fitting of original error data for the X and Y directions, two sinusoids with the frequency $f = \omega/2\pi$ can be obtained. First, the offset between the Y direction sinusoid and the straight line $y = 0$ is ΔR_1, and then, $\Delta\theta_1$ can be calculated with A_1. Then, the ratio between ΔR_1 and $\Delta\theta_1$ for the X direction sinusoid is calculated according to φ_1, and the ratio is brought into A_1 to calculate ΔR_1 and $\Delta\theta_1$ sequentially. A total of six solutions of ΔR_1 and $\Delta\theta_1$ can be obtained. Then, the average values are used as the installation error to compensate.

Similarly, when the machine tool moves in accordance with the XZB motion trajectory, the relative position between the two spheres can be expressed as

$$\begin{cases} \Delta x(t) = -A_2 cos(\omega t - \varphi_2) \\ \Delta y(t) = 0 \\ \Delta z(t) = A_2 sin(\omega t - \varphi_2) - \Delta R_2 \end{cases} \tag{15}$$

where $A_2 = \sqrt{(R_2\Delta\theta_2)^2 + \Delta R_2^2}$ and $\varphi_2 = \arctan\left(\frac{\Delta R_2}{R_2\Delta\theta_2}\right)$.

ΔR_2 and $\Delta\theta_2$ can be calculated by referring to the processing of the XYC motion data. After completing the calculation for the installation errors, the errors are compensated for before measurement.

2.3 Measurement uncertainty

To evaluate the accuracy of the geometric error measured with the DBB, the uncertainty of the geometric error in the X direction is calculated as an example. The geometric error E_{Geo} in the X direction is obtained indirectly by measuring the difference ε between the actual offset distance of the machine tool and the calibration length of the DBB, and it can be expressed as shown in the following equation:

$$\varepsilon = L_M - L_{DBB} \tag{16}$$

where L_M is the machine tool offset distance and L_{DBB} is the calibration length of DBB, ideally $L_{M_ideal} = L_{DBB_ideal} = 50$ mm.

The difference ε includes the ideal difference ε_{ideal} of the DBB, the display error E_{Dis}, and the time drift error E_t, which can be expressed as

$$\varepsilon = \varepsilon_{ideal} + E_{Dis} + E_t \tag{17}$$

The machine tool offset distance L_M includes the geometric error E_{Geo} of the machine tool in the X direction and the installation error E_{In} of the DBB, which can be expressed as

$$L_M = L_{M_ideal} + E_{Geo} + E_{In} \tag{18}$$

The calibration length L_{DBB} of the DBB includes the sphericity error E_{Sp} of the DBB sphere and the calibration ruler error E_{Cali}, which can be expressed as

$$L_{DBB} = L_{DBB_ideal} + E_{Sp} + E_{Cali} \tag{19}$$

Combining the equations, the expression of the geometric error E_{Geo} in the X direction of the machine tool can be obtained as

$$E_{Geo} = f(\varepsilon_{ideal}, E_{Dis}, E_t, E_{In}, E_{Sp}, E_{Cali}) = \varepsilon_{ideal} + E_{Dis} + E_t - E_{In} - E_{Sp} - E_{Cali} \tag{20}$$

The geometric error E_{Geo} includes the display error, time drift error, installation error, and other error terms, so it is necessary to calculate the combined standard uncertainty. The ideal difference ε_{ideal} of the DBB has no error, and its uncertainty is not calculated. The combined standard uncertainty $u(E_{Geo})$ of the geometric error E_{Geo} can be expressed as

$$u^2(E_{Geo}) = c_{E_{Dis}}^2 u^2(E_{Dis}) + c_{E_t}^2 u^2(E_t) + c_{E_{In}}^2 u^2(E_{In}) + c_{E_{Sp}}^2 u^2(E_{Sp}) + c_{E_{Cali}}^2 u^2(E_{Cali}) \tag{21}$$

where $u(E_{Dis})$, $u(E_t)$, $u(E_{In})$, $u(E_{Sp})$, and $u(E_{Cali})$ are uncertainty of each error term, and $c_{E_{Dis}}$, c_{E_t}, $c_{E_{In}}$, $c_{E_{Sp}}$, and $c_{E_{Cali}}$ are the uncertainty coefficients of each error term, which can be obtained by taking the partial derivative with respect to f, $c_{E_{Dis}} = c_{E_t} = 1, c_{E_{In}} = c_{E_{Sp}} = c_{E_{Cali}} = -1$.

In the X direction, the installation error E_{In} includes the four installation errors ΔR_1, $\Delta\theta_1$, ΔR_2, and $\Delta\theta_2$, and the installation error E_{In} in the X direction can be expressed as

$$E_{In} = -R_1\Delta\theta_1\cos\omega t - \Delta R_1\sin\omega t - R_2\Delta\theta_2\cos\omega t - \Delta R_2\sin\omega t \tag{22}$$

The uncertainty $u(E_{In})$ can be expressed as

$$u^2(E_{In}) = c_{\Delta R_1}^2 u^2(\Delta R_1) + c_{\Delta\theta_1}^2 u^2(\Delta\theta_1) + c_{\Delta R_2}^2 u^2(\Delta R_2) + c_{\Delta\theta_2}^2 u^2(\Delta\theta_2) \tag{23}$$

where $c_{\Delta R_1} = c_{\Delta R_2} = -\cos\omega t$, $c_{\Delta\theta_1} = R_1\sin\omega t$, and $c_{\Delta\theta_2} = R_2\sin\omega t$.

The uncertainty calculation is divided into a type A standard uncertainty and a type B standard uncertainty. The type A standard uncertainty is obtained with a limited number of measurements or observations. It is a statistic, and the standard deviation can be calculated as the standard uncertainty. The type B standard uncertainty is obtained from the verification data of reliable testing institutions or manufacturers. The specific calculation method can be determined by referring to reference [33] according to the probability distribution of each term.

3 Geometric error measurement

3.1 Equipment and instrument

The machine tool used in the geometric error measurement experiment is a five-axis ultra-precision machine tool designed and manufactured by the center of precision engineering of Harbin Institute of Technology as illustrated in Fig. 5, with a stroke of 200 mm*100 mm*200 mm. The machine tool adopts the layout shown in Fig. 1.To ensure the machining accuracy, the error motion of the five-axis ultra-precision machine tool within the range of 50 mm*50 mm*50 mm needs to be less than ± 3 μm. To improve the accuracy of the machine tool, the X-, Y-, Z-, and B-axes are all hydrostatic guide rails, and the C-axis is an aerostatic spindle. The bed, X-axis, and Z-axis of the machine tool are made of granite with a small thermal expansion coefficient to avoid thermal errors that have a great impact on the machining accuracy of the machine tool. The measuring instrument is a Renishaw's QC-20W DBB with a resolution of 0.1 μm and a range of ± 1 mm, which can fulfill the measurement requirements.

To avoid the interference of the thermal error with the measurement results, a constant temperature room is built around the machine tool to isolate the influence of the external environmental temperature on the machine tool, as illustrated in Fig. 6a. The interior of the constant temperature room is air-bathed by the precision air conditioner, and four temperature sensors are up to monitor the temperature in the constant temperature room, as shown in Fig. 6c. The

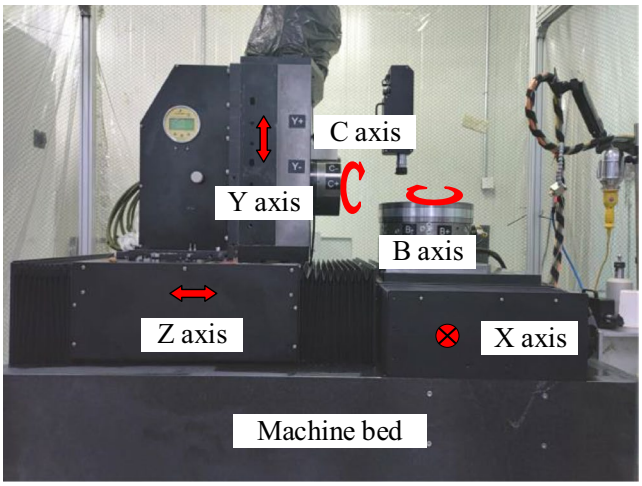

Fig. 5 Five-axis ultra-precision machine tool

temperature change rate is less than ± 0.05 °C/24 h, as demonstrated in Fig. 6d.

Before measurement, it is necessary to turn on the precision air conditioner to air bathe the equipment for more than 7 days to stabilize the internal temperature of the machine tool and the DBB. Since the temperature change rate is less than ± 0.05 °C/24 h, the thermal error in the measurement process is ignored. Additionally, the load error is ignored because the mass of the DBB is much smaller than that of the moving parts of the machine tool.

3.2 Measurement process

3.2.1 DBB installation

First, the two magnetic sockets of the DBB are installed, and their positions are measured. A standard sphere is installed on the *C*-axis, and the *C*-axis rotation axis is measured with the Renishaw touch probe OMP400 with a resolution of ± 0.13 μm, as illustrated in Fig. 7a. Magnetic socket 1 is installed at the end of the fixture, and the distance is offset from the *C*-axis rotation axis. A precision sphere of the same size as the DBB sphere is placed on magnetic socket 1, as illustrated in Fig. 7b. The Renishaw touch probe is used to measure the sphere coordinates, and the offset distance R_1 and the offset angle θ_1 are calculated.

Next, a sharp needle is placed on the *B*-axis, as illustrated in Fig. 8a. The *B*-axis is rotated, CCD camera with a resolution of ± 0.01 μm is used to obtain the trajectory of the needle tip, the center of the trajectory is fitted, and the coordinates of the *B*-axis rotation axis are obtained. Magnetic socket 2 is installed on the *B*-axis, and the precision sphere is placed on magnetic socket 2, as illustrated in Fig. 8b. The CCD camera is used to measure the sphere coordinates, and the offset distance R_2 and the offset angle θ_2 are calculated.

At this point, the installation of the magnetic sockets and the measurement of the coordinates are completed. $R_1 = 24.4985$ mm, $\theta_1 = 24.3681°$, $R_2 = 23.5697$ mm, and $\theta_2 = 1.6073°$. The *C*-axis and the *B*-axis are rotated through θ_1 and θ_2, respectively, and then, the angle at this time is defined as 0° in the program coordinate system.

The linear axes are moved so that the coordinates of sphere 1 and sphere 2 coincide in the machine tool coordinate, and then, the *X*-axis is moved in the positive direction by 50 mm. This point is set as the program zero point, and the DBB is installed as illustrated in Fig. 9a. The *Y*-axis and *Z*-axis are reciprocated to observe whether the DBB indication is the smallest at the zero point. If the DBB indication is the smallest at the zero point, the DBB installation toward *X* direction is completed, and the error measurement work has begun. If the minimum indication appears outside the zero point, then the coordinates of the *B*-axis, the *C*-axis rotation axes, and the magnetic sockets are re-measured. The installation method for the *Y* direction and the *Z* direction is similar to that for the *X* direction.

3.2.2 Measurement of installation errors

After completing the installation work, the installation errors of the DBB are measured. First, the DBB toward the *X* direction is installed, and R_1 is brought into the Eq. (9) to generate the NC program. The NC program is executed, and the error values are measured during the progress. The measurement is repeated three times to obtain the error curves as illustrated in Fig. 10a, and then, the DBB toward the *Y* direction is installed. The error curves shown in Fig. 10b are obtained. In the experiment for the measurement of the installation errors, the *C*-axis speed is 2.76° per second, the program running time is 130 s, and the DBB sampling frequency is 13.889 Hz.

It can be observed from the curves in Fig. 10 that the measurement results have a good repeatability, so the first measured data are taken for sinusoidal fitting, and the sinusoid of the *X* direction error curves is obtained:

$$\Delta x(t) = -0.0121 \cdot \cos(\omega t + 21.9199°)$$

The sinusoid of the *Y* direction error curves is

$$\Delta y(t) = 0.0120 \cdot \cos(\omega t - 69.2323°) - 0.00460$$

Then, the sinusoid of the *Y* direction error curves is deformed based on the trigonometric function:

$$\Delta y(t) = 0.0120 \cdot \sin(\omega t + 20.7677°) - 0.00460$$

The sinusoids of the *X* direction and the *Y* direction are compared. It can be found that the amplitudes and phase angles of the two are approximately equal, so the installation

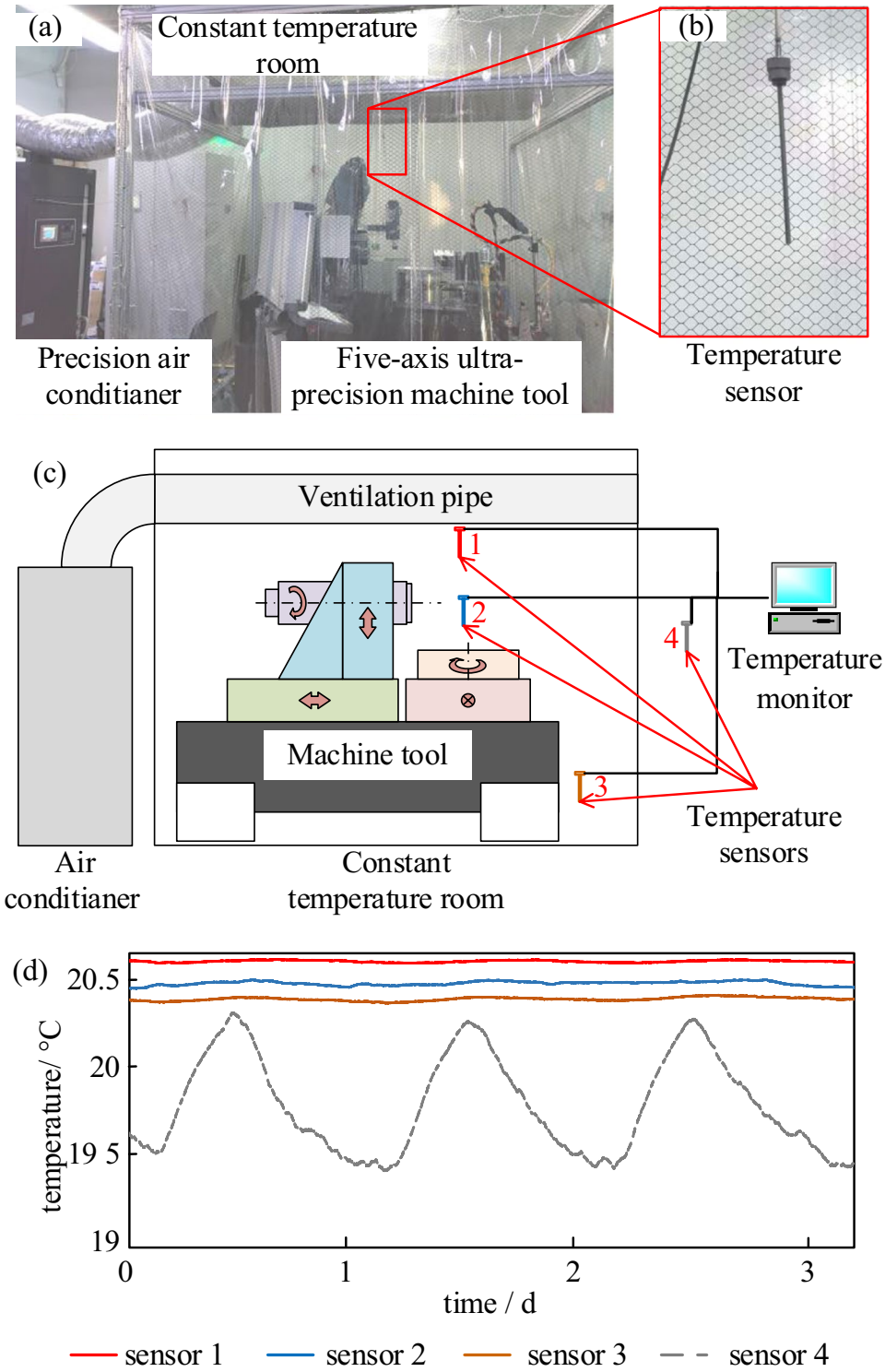

Fig. 6 Constant temperature room: **a** constant temperature room, **b** temperature sensor, **c** schematic diagram of temperature monitoring, and **d** temperature curves

errors are the main component in the fundamental frequency signal of the error curves. The calculation is performed according to the original data. The calculation results of ΔR_1 and $\Delta\theta_1$ are shown in Table 1. Taking the average values, the installation errors are $\Delta R_1 = 0.0046$ mm and $\Delta\theta_1 = 0.00046°$.

Similarly, by running the XZB three-axis NC program, the error curves illustrated in Fig. 11 can be obtained.

In accordance with the curves in Fig. 11, the calculation results of ΔR_2 and $\Delta\theta_2$ are listed in Table 2; taking the average values, the installation errors are $\Delta R_2 = 0.0063$ mm and $\Delta\theta_2 = 0.00013°$.

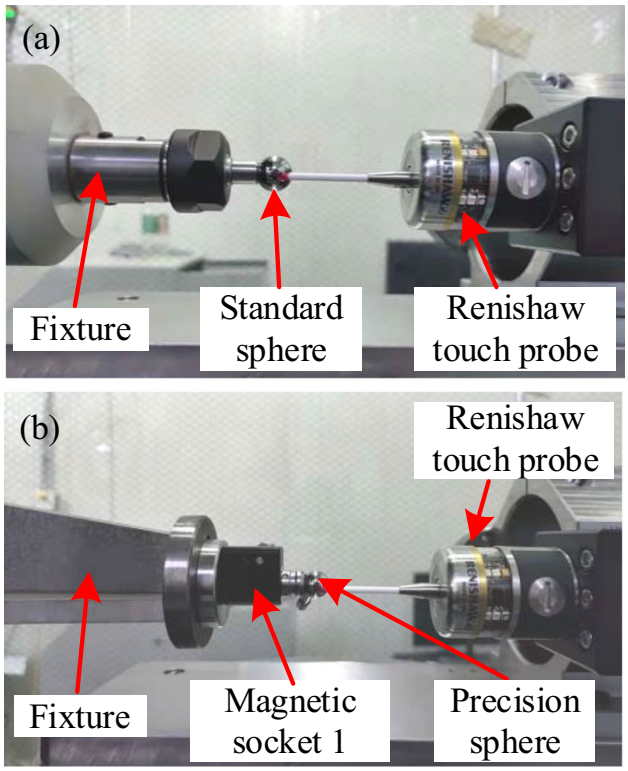

Fig. 7 Magnetic socket 1 installation: **a** *C*-axis rotation axis measurement. **b** Precision sphere coordinate measurement

At this point, the measurement and the calculation of all installation errors are completed. The compensated rotational radii are $R_1 = 24.5031$ mm and $R_2 = 23.5760$ mm. The compensated R_1 and R_2 are brought into Eq. (3), and the NC program can be generated. The NC program is executed, and the DBB is used to measure the geometric errors of the machine tool. The measurement is repeated three times. In the experiment, the rotational speeds of the *C*-axis and the *B*-axis are both 2.83° per second, the program running time is 127 s, and the DBB sampling frequency is 13.889 Hz.

4 Result and discussion

4.1 Measurement result and theoretical result

The five-axis NC program is executed, and the DBB is used to measure the errors of motion along the test trajectory to obtain the error curves, as illustrated in Fig. 12.

As shown in Fig. 12, the three measurement results have a good repeatability, the δ_x are 2.5 μm, 2.4 μm, and 2.4 μm; the δ_y are 3.7 μm, 3.6 μm, and 3.6 μm; and the δ_z are 2.9 μm, 3.1 μm, and 3.1 μm. The average value of total error δ is 5.26 μm, which equals to ± 2.63 μm.

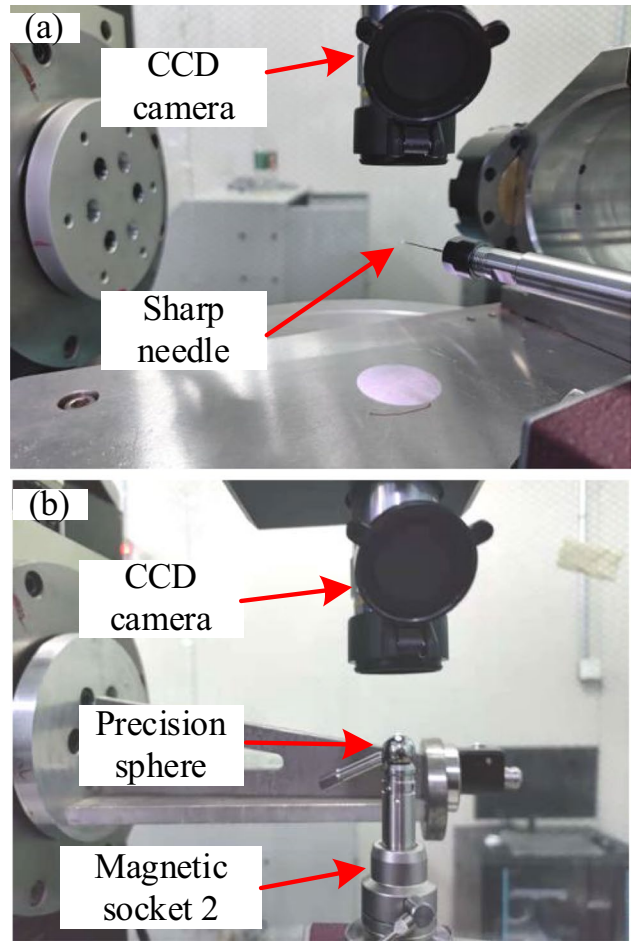

Fig. 8 Magnetic socket 2 installation: **a** *B*-axis rotation axis measurement. **b** Precision sphere coordinate measurement

The geometric error model of the machine tool is established by using the multi-body system theory, and the accuracy of the error measurement results is analyzed. In accordance with ISO 230–1 [2] and ISO 230–7[34], the 43 geometric error terms of the five-axis ultra-precision machine tool are listed in Table 3.

The five-axis machine tool has three linear axes, which can realize the translation of the *B*-axis and the *C*-axis; thus, the position errors can be compensated by calibration in advance. Therefore, the position errors E_{XOB}, E_{ZOB}, E_{XOC}, and E_{YOC} can be ignored, and the initial angles of the *B*-axis and the *C*-axis are redefined in the NC program, so the zero angle position errors E_{BOB} and E_{COB} are ignored. Therefore, this research mainly studies the remaining 37 error terms.

In multi-body system theory, a 4 × 4 homogeneous transformation matrix is generally used to describe coordinate transformation in space. The error matrix in the static or moving state between adjacent axes can be obtained by multiplying the basic error matrix. Because only the geometric error of the machine tool is considered in this

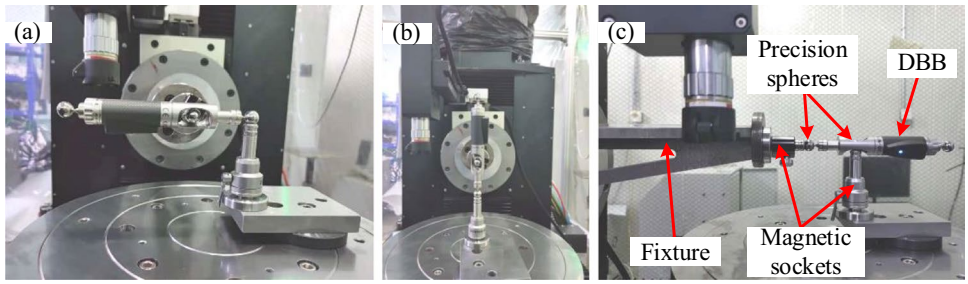

Fig. 9 DBB installation: **a** *X* direction, **b** *Y* direction, and **c** *Z* direction

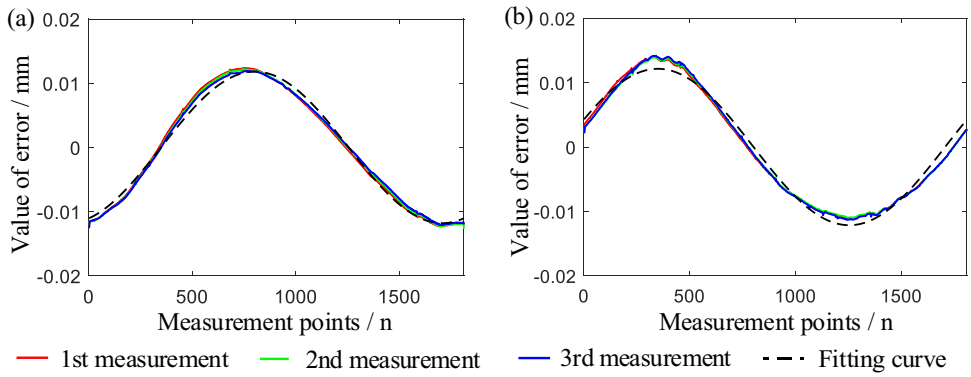

Fig. 10 Error curves in XYC-axis motion: **a** *X* direction error curves. **b** *Y* direction error curves

Table 1 The ΔR_1 and the $\Delta\theta_1$ values

Terms	Values	Mean
ΔR_1 (mm)	0.0046, 0.0045, 0.0046, 0.0046, 0.0046, 0.0045	0.0046
$\Delta\theta_1$ (°)	0.000454, 0.000456, 0.000453, 0.000464, 0.000463, 0.000461	0.00046

study and attention is not paid to the installation error of the tool and workpiece, the homogeneous transformation matrixes between the *C*-axis and workpiece as well as the *B*-axis and tool are unit matrixes. The ideal static state transformation matrix and the real static state transformation matrix between adjacent axes are listed in Table 4. The ideal motion state transformation matrix and the real motion state transformation matrix between adjacent axes are listed in Table 5.

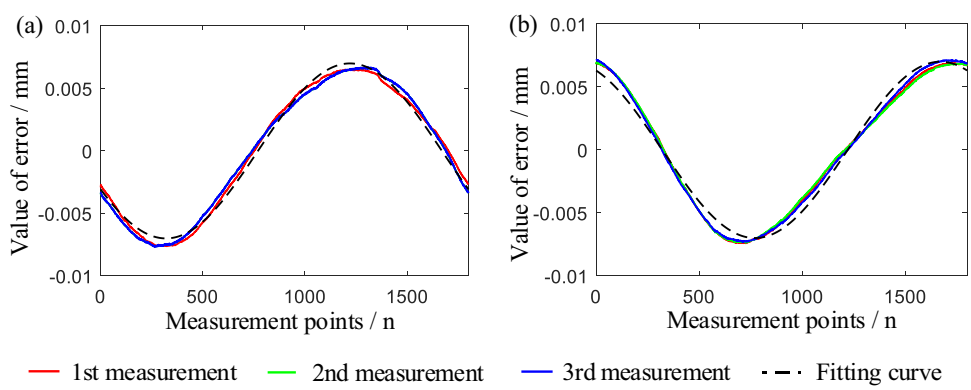

Fig. 11 Error curves in XZB-axis motion: **a** *X* direction error curves. **b** *Z* direction error curves

Table 2 The ΔR_2 and the $\Delta\theta_2$ values

Terms	Values	Mean
ΔR_2 (mm)	0.0063, 0.0062, 0.0062, 0.0063, 0.0062, 0.0063	0.0063
$\Delta\theta_2$ (°)	0.000131, 0.000134, 0.000133, 0.000129, 0.000127, 0.000131	0.00013

When the five-axis ultra-precision machine tool has no error, the measuring point trajectory is consistent with the ideal trajectory, and the real measuring point is consistent with the ideal measuring point. Assume that the coordinate of the measuring point along the tool path is $P_t = [P_{tx}, P_{ty}, P_{tz}, 1]^T$, the coordinate of the measuring point along the

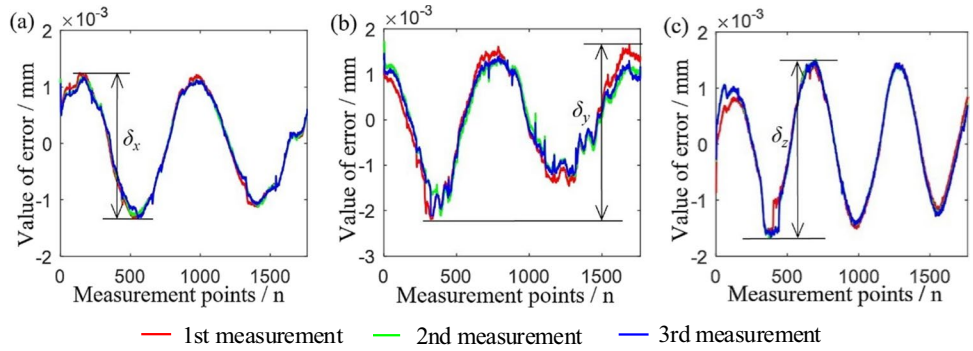

Fig. 12 Error curves in five-axis motion: **a** *X* direction error curves, **b** *Y* direction error curves, and **c** *Z* direction error curves

Table 3 Error terms of five-axis ultra-precision machine tool

Axis	Error terms
X-axis	$^{*}E_{XX}$, E_{YX}, E_{ZX}, E_{AX}, E_{BX}, E_{CX}
Y-axis	E_{XY}, $^{*}E_{YY}$, E_{ZY}, E_{AY}, E_{BY}, E_{CY}
Z-axis	E_{XZ}, E_{YZ}, $^{*}E_{ZZ}$, E_{AZ}, E_{BZ}, E_{CZ}
B-axis	E_{XB}, E_{YB}, E_{ZB}, E_{AB}, $^{*}E_{BB}$, E_{CB}, E_{XOB}, E_{ZOB}, E_{BOB}
C-axis	E_{XC}, E_{YC}, E_{ZC}, E_{AC}, E_{BC}, $^{*}E_{CC}$, E_{XOC}, E_{YOC}, E_{COC}
Squareness errors	E_{BOX}, E_{AOY}, E_{COY}, E_{AOC}, E_{BOC}, E_{AOB}, E_{COB}

*are the positioning errors, and the rest are the geometric errors

workpiece is $P_w = [P_{wx}, P_{wy}, P_{wz}, 1]^T$, and the ideal measuring point along the workpiece P_{w_ideal} can be calculated with the following equation:

$$\left[\prod_{i=1}^{4} T_{ip}T_{is}\right] P_{w_ideal} = \left[\prod_{j=5}^{7} T_{jp}T_{js}\right] P_t \tag{24}$$

For the tool coordinate, the ideal measuring point along the workpiece P_{w_ideal} can be expressed as

$$P_{w_ideal} = \left[\prod_{i=1}^{4} T_{ip}T_{is}\right]^{-1} \left[\prod_{j=5}^{7} T_{jp}T_{js}\right] P_t \tag{25}$$

In the real machining process, due to the 37 geometric error terms in the five-axis ultra-precision machine tool, for the tool coordinate, the real measuring point along the workpiece P_{w_real} can be expressed as

$$P_{w_real} = \left[\prod_{i=1}^{4} T_{ip}\Delta T_{ip}T_{is}\Delta T_{is}\right]^{-1} \cdot \left[\prod_{j=5}^{7} T_{jp}\Delta T_{jp}T_{js}\Delta T_{js}\right] P_t \tag{26}$$

Table 4 Static state transformation matrix between adjacent axes

Adjacent axes	Ideal transformation matrix	Real transformation matrix
Bed–*Z*-axis	$T_{1p} = I_{4\times4}$	$\Delta T_{1p} = I_{4\times4}$
Z-axis–*Y*-axis	$T_{2p} = I_{4\times4}$	$\Delta T_{2p} = \begin{bmatrix} 1 & -E_{AOY} & 0 & 0 \\ E_{AOY} & 1 & -E_{COY} & 0 \\ 0 & E_{COY} & 1 & 0 \\ 0 & 0 & 0 & 1 \end{bmatrix}$
Y-axis–*C*-axis	$T_{3p} = I_{4\times4}$	$\Delta T_{3p} = \begin{bmatrix} 1 & 0 & E_{AOC} & 0 \\ -E_{AOC} & 1 & -E_{BOC} & 0 \\ 0 & E_{BOC} & 1 & 0 \\ 0 & 0 & 0 & 1 \end{bmatrix}$
C-axis–workpiece	$T_{4p} = I_{4\times4}$	$\Delta T_{4p} = I_{4\times4}$
Bed–*X*-axis	$T_{5p} = I_{4\times4}$	$\Delta T_{5p} = \begin{bmatrix} 1 & 0 & E_{BOX} & 0 \\ 0 & 1 & 0 & 0 \\ -E_{BOX} & 0 & 1 & 0 \\ 0 & 0 & 0 & 1 \end{bmatrix}$
X-axis–*B*-axis	$T_{6p} = I_{4\times4}$	$\Delta T_{6p} = \begin{bmatrix} 1 & -E_{AOB} & 0 & 0 \\ E_{AOB} & 1 & -E_{COB} & 0 \\ 0 & E_{COB} & 1 & 0 \\ 0 & 0 & 0 & 1 \end{bmatrix}$
B-axis–tool	$T_{7p} = I_{4\times4}$	$\Delta T_{7p} = I_{4\times4}$

Table 5 Motion state transformation matrix between adjacent axes

Adjacent axes	Ideal transformation matrix	Real transformation matrix
Bed–*Z*-axis	$T_{1S}=\begin{bmatrix}1&0&0&0\\0&1&0&0\\0&0&1&Z\\0&0&0&1\end{bmatrix}$	$\Delta T_{1S}=\begin{bmatrix}1&-E_{CZ}&E_{BZ}&E_{XZ}\\E_{CZ}&1&-E_{AZ}&E_{YZ}\\-E_{BZ}&E_{AZ}&1&E_{ZZ}\\0&0&0&1\end{bmatrix}$
Z-axis–*Y*-axis	$T_{2S}=\begin{bmatrix}1&0&0&0\\0&1&0&Y\\0&0&1&0\\0&0&0&1\end{bmatrix}$	$\Delta T_{2S}=\begin{bmatrix}1&-E_{CY}&E_{BY}&E_{XY}\\E_{CY}&1&-E_{AY}&E_{YY}\\-E_{BY}&E_{AY}&1&E_{ZY}\\0&0&0&1\end{bmatrix}$
Y-axis–*C*-axis	$T_{3S}=\begin{bmatrix}\cos C&-\sin C&0&0\\\sin C&\cos C&0&0\\0&0&1&0\\0&0&0&1\end{bmatrix}$	$\Delta T_{3S}=\begin{bmatrix}1&-E_{CC}&E_{BC}&E_{XC}\\E_{CC}&1&-E_{AC}&E_{XC}\\-E_{BC}&E_{AC}&1&E_{ZC}\\0&0&0&1\end{bmatrix}$
C-axis–workpiece	$T_{4S}=I_{4\times4}$	$\Delta T_{4S}=I_{4\times4}$
Bed–*X*-axis	$T_{5S}=\begin{bmatrix}1&0&0&X\\0&1&0&0\\0&0&1&0\\0&0&0&1\end{bmatrix}$	$\Delta T_{5S}=\begin{bmatrix}1&-E_{CX}&E_{BX}&E_{XX}\\E_{CX}&1&-E_{AX}&E_{YX}\\-E_{BX}&E_{AX}&1&E_{ZX}\\0&0&0&1\end{bmatrix}$
X-axis–*B*-axis	$T_{6S}=\begin{bmatrix}\cos B&0&\sin B&0\\0&1&0&0\\-\sin B&0&\cos B&0\\0&0&0&1\end{bmatrix}$	$\Delta T_{6S}=\begin{bmatrix}1&-E_{CB}&E_{BB}&E_{XB}\\E_{CB}&1&-E_{AB}&E_{YB}\\-E_{BB}&E_{AB}&1&E_{ZB}\\0&0&0&1\end{bmatrix}$
B-axis–tool	$T_{7S}=I_{4\times4}$	$\Delta T_{7S}=I_{4\times4}$

The resultant error E at the measuring point can be considered as the difference between the P_{w_real} and the P_{w_ideal}, which can be calculated with the following equation:

$$E=[E_x,E_y,E_z,1]^{\mathrm{T}}=P_{w_real}-P_{w_ideal} \tag{27}$$

where E_x, E_y, and E_z are the error components of the resultant error E in the X, Y, and Z directions.

Thirty-seven geometric error terms of the five-axis ultra-precision machine tool are measured. Part of the measurement process is demonstrated in Fig. 13. The values of each error term are listed in Table 6.

The 37 geometric error terms and the test trajectory are brought into the machine tool error model, and the theoretical curves of the resultant errors in the X, Y, and Z directions by the interpolated five-axis motion are obtained. These curves are compared with the measurement curves in Fig. 14.

From Fig. 14, it can be found that the tendencies of the theoretical curves and measurement curves are generally consistent. The PV values of the theoretical errors in the X, Y, and Z directions are 2.2 μm, 3.4 μm, and 2.8 μm, and the total error δ is 4.92 μm, which is equal to $\pm$2.46 μm. The differences between the PV values and the total error of theoretical results and measurement results are less than 0.4 μm, which shows good agreement, but there is a large deviation in some areas.

In this research, the error model based on the multi-body system theory is used to calculate the resultant errors of the test trajectory. The tendency, the PV values, and the total error δ of the theoretical results and the measurement results are basically consistent, indicating that the DBB can be used to accurately measure the geometric error of the machine tool. This also proves that the geometric error model of the machine tool established with the multi-body system theory has high reliability and can be used to evaluate the geometry error of the five-axis ultra-precision machine tool.

The reasons for the theoretical curves are not as regular as the measurement curve in the beginning and end areas are as follows:

(1) *The dynamic error of the machine tool*. In the multi-body system theory, only the geometric error of the machine tool is considered, and the dynamic error is not involved. In the measurement process, the geometric error and the dynamic error of the machine tool are both included in the result.

The dynamic errors include the response delays and servo mismatches. The motion speed can be obtained with the derivation of the motion trajectory. When $t=0$, the speed in the X direction suddenly accelerates from 0 to $-(R_1+R_2)$, while the speeds in the Y and Z directions are still 0. The X-axis motor cannot complete the response in such a short time, so there is a large deviation between the theoretical

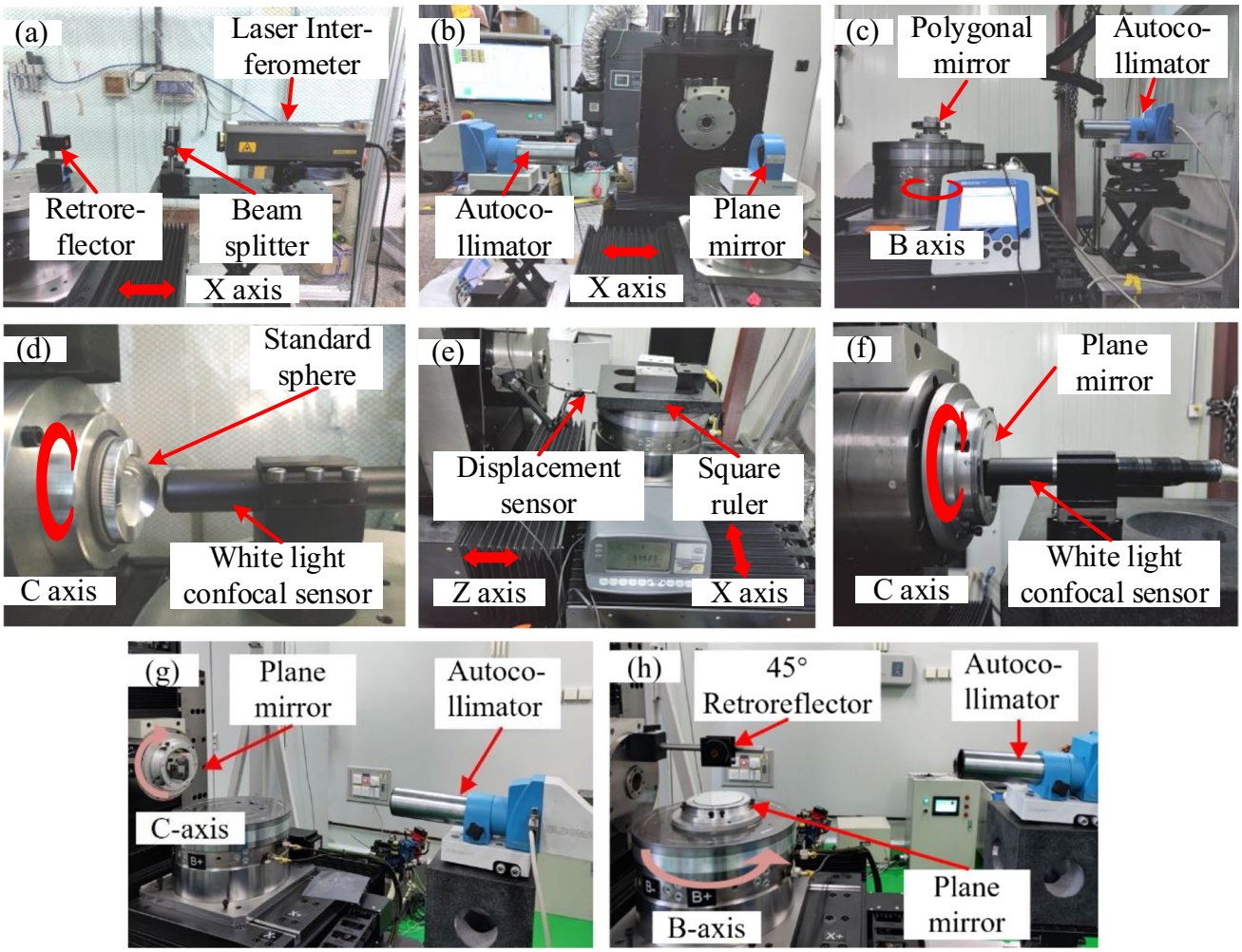

Fig. 13 Measurement of geometric error terms: **a** *X*-axis positioning error, **b** *X*-axis straightness error, **c** *B*-axis positioning error, **d** *C*-axis rotation error, **e** squareness error between *X*-axis and *Z*-axis, and **f** squareness error between *C*-axis and *X*-axis, **g** *C*-axis orientation errors, and **h** *B*-axis orientation errors

Table 6 Measured values of 37 error terms

Error term	Value/μm	Error term	Value/μm	Error term	Value/″	Error term	Value/″
E_{XX}	0.55	E_{ZB}	0.06	E_{AX}	0.60	E_{CB}	0.19
E_{YX}	0.17	E_{XC}	0.03	E_{BX}	0.61	E_{AC}	0.18
E_{ZX}	0.11	E_{YC}	0.03	E_{CX}	1.10	E_{BC}	0.12
E_{XY}	0.01	E_{ZC}	0.02	E_{AY}	1.03	E_{CC}	1.22
E_{YY}	0.47			E_{BY}	0.12	E_{XOZ}	0.83
E_{ZY}	0.12			E_{CY}	0.08	E_{YOZ}	0.70
E_{XZ}	0.03			E_{AZ}	1.33	E_{YOX}	0.73
E_{YZ}	0.16			E_{BZ}	0.42	E_{COX}	-0.27
E_{ZZ}	0.38			E_{CZ}	0.19	E_{COY}	0.60
E_{XB}	0.06			E_{AB}	0.18	E_{BOX}	-0.38
E_{YB}	0.05			E_{BB}	1.12	E_{BOZ}	0.55

results and the measurement results in the *X* direction near the time $t=0$, and the deviation between the *Y* direction and the *Z* direction is small.

(2) *Instrument time drift error*. In the measurement experiment, at the end of the NC program, the indication of the DBB sometimes changes from 50.0000 to 50.0002 mm

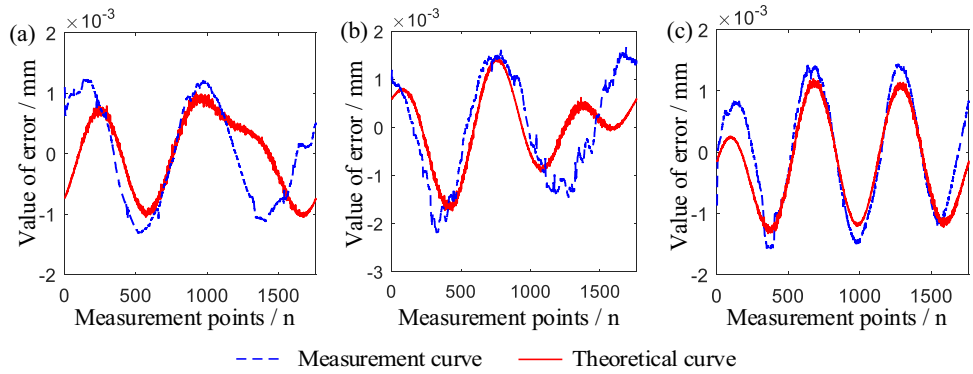

Fig. 14 Error curves comparison between theory and measurement: **a** *X* direction, **b** *Y* direction, and **c** *Z* direction

or 50.0004 mm, which is an increase of 0.2 − 0.3 μm. The increased length may be the time drift error of the DBB. The existence of the time drift error of the DBB causes the deviation between the theoretical results and the measurement results to gradually increase with time, so the deviation in the end area of the curve is significantly larger than that in the initial area.

(3) *Machine tool structure*. In ultra-precision machine tools, an unloading cylinder is generally used to balance the mass of the *Y*-axis slider and the *C*-axis. The connection between the *Y*-axis slide and the unloading cylinder of the five-axis ultra-precision machine tool used in this experiment is a ball joint. Due to the manufacturing error of the ball joint, there is backlash when the *Y*-axis reciprocates. In addition, when the *Y*-axis moves downward, the unloading cylinder is in the exhaust state, and when the *Y*-axis moves upward, the unloading cylinder is in the suction state. When the movement direction of the *Y*-axis changes, due to the existence of air damping, the unloading cylinder cannot switch the operating state quickly. These two factors lead to the backlash error when the *Y*-axis reciprocates.

As shown in Fig. 14b, after the 1000th measurement point, the deviation between the theoretical results and measurements result begins to increase, corresponding to the change of the movement direction of the *Y*-axis. Therefore, this part of the deviation may be caused by the backlash when the *Y*-axis reciprocates. When the unloading cylinder structure is used in the *Y*-axis, the position and the movement direction of the *Y*-axis should be kept unchanged during the machining process. If the *Y*-axis reciprocating motion is genuinely required, the *Y*-axis movement speed should be reduced to avoid large geometric tolerances for the workpiece.

In addition, in the measurement process, the machine tool is affected by external vibration, the fluctuations of air pressure and oil pressure, so the measurement curves are not as regular as the theoretical curves.

4.2 Measurement uncertainty calculation

The resolution of the DBB is 0.1 μm, the display error E_{Dis} has a rectangular distribution, and equal probability lies within (−0.05, 0.05), with associated variance

$$u\left(E_{Dis}\right)^2 = 0.1^2/12 = 0.00083\mu m^2$$

The standard uncertainty of the display error E_{Dis} is

$$u\left(E_{Dis}\right) = 0.029\mu m$$

E_t is the time drift error of the DBB, which increases with the measurement time and presents a rectangular distribution. In 21 measurement experiments, the maximum value is 0.3 μm, and the degrees of freedom is 20. By checking the Appendix Table E.1 in reference [33], it is determined that the inclusion probability is 84%. The standard uncertainty of the time drift error E_t is

$$u\left(E_t\right) = 0.3/\sqrt{3} = 0.173\mu m$$

The installation errors ΔR_1, $\Delta\theta_1$, ΔR_2, and $\Delta\theta_2$ are obtained with a limited number of measurements categorized as type A standard uncertainty, so the standard deviation is calculated as the standard uncertainty. According to the discussion in Sect. 3.2.2, the standard deviation of ΔR_1 is 0.051 μm, the standard deviation of $\Delta\theta_1$ is 0.0000043°, the standard deviation of ΔR_2 is 0.040 μm, and the standard deviation of $\Delta\theta_2$ is 0.0000023°. Taking sin ωt = cos

$\omega t = 1$, the standard uncertainty of the installation error E_{In} is

$$u^2(E_{In}) = 0.051^2 + 24503.1^2 \cdot 0.0000043^2 + 0.04^2 + 23576^2 \cdot 0.0000023^2 = 0.0182\mu m^2$$

or $u(E_{In}) = 0.134\mu m$

The diameter of the DBB sphere is 12.7 mm, and the diameter of the contact area between the magnetic socket and sphere is 8 mm. According to the geometric relationship, the error coefficient caused by the sphericity error E_{Sp} in the length direction is 8/12.7 = 0.63. The precision level of the DBB sphere is AFBMA10. The sphericity error is less than 0.15 μm, and it is normally distributed. The inclusion probability is 99%. By checking the Appendix Table G.2 in reference [33], using the t factor $t_{99}(\infty) = 2.576$, it is determined that the standard uncertainty of the sphericity error E_{Sp} is

$$u(E_{Sp}) = 0.63 \cdot 0.15/2.576 = 0.037\mu m$$

The calibration ruler error E_{Cali} is less than 0.1 μm, with a normal distribution, and the inclusion probability is 99%. Using the t factor $t_{99}(\infty) = 2.576$, the standard uncertainty of the calibration ruler error E_{Cali} is

$$u(E_{Cali}) = 0.1/2.576 = 0.039\mu m$$

In summary, the combined standard uncertainty of the geometric error in the X direction is

$$u^2(\varepsilon) = 0.029^2 + 0.173^2 + 0.134^2 + 0.037^2 + 0.039^2 = 0.052\mu m^2$$

or $u(\varepsilon) = 0.227\mu m$

After calculation, the standard uncertainty of the X direction geometric error is determined to be 0.227 μm, and the relative uncertainty is determined to be 0.077. Similarly, the standard uncertainty of the Y direction geometric error is 0.175 μm, and the relative uncertainty is 0.048, the standard uncertainty of the Z direction geometric error is 0.022 μm, and the relative uncertainty is 0.007.

According to the measurement uncertainty calculation, the uncertainty of the geometric error is less than 0.2 μm, and the relative uncertainty is less than 0.1, which proves that the measurement results are credible. At the same time, according to the calculation process, the time drift error E_t and the installation error E_{In} account for a large proportion of the uncertainty. Therefore, a faster running speed should be chosen, and the measurement time should be decreased to reduce the influence of the time drift error E_t. Additionally, when measuring the installation error, measurement equipment with higher accuracy should be selected as often as possible or the number of measurements should be increased to reduce the uncertainty of the installation error E_{In}.

In this research, a new measurement method is proposed that uses a DBB to measure the geometric error of a five-axis ultra-precision machine tool in the interpolated five-axis motion. Although the deviation is large in some areas, the tendency, the PV values, and the total error of the theoretical results and the measurement results are basically consistent. The difference between the PV values and the total error is less than 0.4 μm.

It is proven that the DBB can accurately measure the geometric error of the five-axis ultra-precision machine tool, and this method can be used as a more stringent measurement method to measure the geometric error of the machine tool. When the geometric error measured with this method meets the design index, the accuracy of the machine tool can be considered qualified.

At the same time, the method in this research can be used to complete the geometric error measurement of the five-axis machine tool effectively using only a DBB, and it is simpler than the traditional method. In addition, the large deviation in some areas also reflects the limitation of the multi-body system theory. In follow-up research, the theory needs to be further optimized, and the dynamic error part needs to be added to the multi-body system theory to make it closer to the error situation of machine tools.

5 Conclusions

In this paper, a measurement method based on the DBB is proposed that can measure the geometric error of a five-axis ultra-precision machine tool, and the measurement experiments are carried out using a five-axis ultra-precision machine tool with a *w–C-Y–Z-b-X-B-t* layout. The method can be used to measure the resultant errors in the X, Y, and Z directions of a five-axis ultra-precision machine tool by only one measurement equipment and one-time installation. Compared with the measurement methods mentioned in the ISO 230–1, the method proposed in this research is less limited by the layout of machine tools and can be used to perform the error measurement for five-axis ultra-precision machine tools.

Acknowledgements We appreciate the invaluable expert comments and advice on the paper from all anonymous reviewers.

Author contribution Luqi Song: methodology; validation; formal analysis; investigation; data curation; writing-original draft preparation; writing-review and editing. Xueshen Zhao: methodology, validation, formal analysis, investigation, data curation. Qiang Zhang: methodology investigation; investigation; project administration. Dequan Shi: conceptualization; methodology; formal analysis; investigation;

supervision; project administration. Tao Sun: generation of project ideas; conceptualization; methodology; validation; investigation; writing-review and editing; project administration; funding acquisition.

Funding This work was supported by the Science Challenge Project of China [Grant No. TZ2018006-0202–01].

Availability of data and material The authors confirm that the data supporting the findings of this study are available within the article.

Code availability Not applicable.

Declarations

Ethics approval The article involves no studies on human or animal subjects.

Consent to participate All authors were fully involved in the study and preparation of the manuscript, and each of the authors has read and concurred with the content in the final manuscript.

Consent for publication All authors consent to publish the content in the final manuscript.

Competing interests The authors declare no competing interests.

Disclaimer The authors do not have any commercial or associative interest that represents a conflict of interest in connection with the work submitted.

References

1. Schwenke H, Knapp W, Haitjema H, Weckenmann A, Schmitt R, Delbressine F (2008) Geometric error measurement and compensation of machines-an update. CIRP Ann - Manuf Technol 57:660–675
2. International Organization For Standardization (2012) ISO 230-1 Test code for machine tools - Part 1: Geometric accuracy of machines operating under no-load or quasi-static conditions
3. Wang H, Ran Y, Zhang S, Li Y (2020) Coupling and decoupling measurement method of complete geometric errors for multi-axis machine tools. Appl Sci 10:2164
4. Liu X, Zhang X, Fang F, Liu S (2016) Identification and compensation of main machining errors on surface form accuracy in ultra-precision diamond turning. Int J Mach Tools Manuf 105:45–57
5. Ibaraki S, Knapp W (2012) Indirect measurement of volumetric accuracy for three-axis and five-axis machine tools: a review. Int J Autom Technol 6:110–124
6. Gao W, Weng L, Zhang J, Tian W, Zhang G, Zheng Y, Li J (2020) An improved machine tool volumetric error compensation method based on linear and squareness error correction method. Int J Adv Manuf Technol 106:4731–4744
7. Wang J, Wang Q, Li H (2019) The method of geometric error measurement of NC machine tool based on the principle of space vector's direction measurement. Int J Precis Eng Manuf 20:511–524
8. Li K, Kuang C, Liu X (2013) Small angular displacement measurement based on an autocollimator and a common-path compensation principle. Rev Sci Instrum 84:015108
9. Ibaraki S, Oyama C, Otsubo H (2011) Construction of an error map of rotary axes on a five-axis machining center by static R-test. Int J Mach Tools Manuf 51:190–200
10. Ibaraki S, Iritani T, Matsushita T (2013) Error map construction for rotary axes on five-axis machine tools by on-the-machine measurement using a touch-trigger probe. Int J Mach Tools Manuf 68:21–29
11. Jiang Z, Song B, Zhou X, Tang X, Zheng S (2015) Single setup identification of component errors for rotary axes on five-axis machine tools based on pre-layout of target points and shift of measuring reference. Int J Mach Tools Manuf 98:1–11
12. Chen Q, Li W, Jiang C, Zhou Z, Min S (2021) Separation and compensation of geometric errors of rotary axis in 5-axis ultra-precision machine tool by empirical mode decomposition method. J Manuf Process 68:1509–1523
13. Ni Y, Liu X, Zhang B, Zhang Z, Li J (2018) Geometric error measurement and identification for rotational axes of a five-axis CNC machine tool. J Mech Eng 64:290–302
14. Dobosz M, Jankowski M, Mruk J (2019) Application of interference sensor of angular micro-displacement in measurements of machine rotational errors. Precis Eng 60:12–20
15. Lai T, Peng X, Tie G, Liu J, Guo M (2017) High accurate squareness measurement squareness method for ultra-precision machine based on error separation. Precis Eng 49:15–23
16. International Organization For Standardization (2002) ISO 230-6 Test code for machine tools - Part 6: Determination of positioning accuracy on body and face diagonals (Diagonal displacement tests)
17. Chapman MAV (2003) Limitations of laser diagonal measurements. Precis Eng 27:401–406
18. Ibaraki S, Hata T (2010) A new formulation of laser step diagonal measurement-three-dimensional case. Precis Eng 34:516–525
19. Sun G, He G, Zhang D, Yao C, Tian W (2020) Body diagonal error measurement and evaluation of a multiaxis machine tool using a multibeam laser interferometer. Int J Adv Manuf Technol 107:4545–4559
20. Yang S, Lee H, Lee K (2018) Face- and body-diagonal length tests using a double ball-bar for squareness errors of machine tools. Int J Precis Eng Manuf 19:1039–1045
21. Kim T, Dunningham J, Burnett K (2005) Precision measurement scheme using a quantum interferometer. Phys Rev A - At Mol Opt Phys 72:1–4
22. Hong C, Ibaraki S (2013) Non-contact R-test with laser displacement sensors for error calibration of five-axis machine tools. Precis Eng 37:159–171
23. Wang W, Chen Z, Zhu Y, Yang H, Lu K, Shi G, Xiang K, Ju B (2020) Full-scale measurement of CNC machine tools. Int J Adv Manuf Technol 107(5–6):2291–2301
24. Lamikiz A, López de Lacalle LN, Celaya A (2009) Machine Tool Performance and Precision. In: López de Lacalle LN, Lamikiz A (eds) Machine Tools for High Performance Machining. Springer, London, pp 219–260
25. International Organization For Standardization (2020) ISO 10791-7 Test conditions for machining centers - Part 7: Accuracy of finished test pieces
26. Fu M, Guan L, Wang L, Mo J, Zhao X (2021) Tool diameter optimization in S-shaped test piece machining. Adv Mech Eng 13:1–8
27. Ibaraki S, Sawada M, Matsubara A, Matsushita T (2010) Machining tests to identify kinematic errors on five-axis machine tools. Precis Eng 34:387–398
28. Ibaraki S, Yoshida I (2017) A five-axis machining error simulator for rotary-axis geometric errors using commercial machining simulation software. Int J Autom Technol 11:179–187

29. Ibaraki S, Yoshida I, Asano T (2019) A machining test to identify rotary axis geometric errors on a five-axis machine tool with a swiveling rotary table for turning operations. Precis Eng 55:22–32
30. Chu W, Zhu S, Peng Y, Ding G (2011) Geometric error identification and compensation for rotation axes of five-axis machine tools. Adv Mater Res 338:786–791
31. Wang Z, Li J (2017) A new decoupling measurement method of five-axis machine tools' geometric errors based on cross grid encoder and DBB. Int Conf Mech Des Manuf Autom. https://doi.org/10.12783/dtetr/mdm2016/4944
32. Chen D, Zhang S, Pan R, Fan J (2018) An identifying method with considering coupling relationship of geometric errors parameters of machine tools. J Manuf Process 36:535–549
33. International Organization For Standardization (2008) ISO/ICE Guide 98-3 Uncertainty of measurement - Part 3: Guide to the expression of uncertainty in measurement
34. International Organization For Standardization (2015) ISO 230-7, Test code for machine tools - Part 7: Geometric accuracy of axes of rotation

Publisher's Note Springer Nature remains neutral with regard to jurisdictional claims in published maps and institutional affiliations.

Springer Nature or its licensor (e.g. a society or other partner) holds exclusive rights to this article under a publishing agreement with the author(s) or other rightsholder(s); author self-archiving of the accepted manuscript version of this article is solely governed by the terms of such publishing agreement and applicable law.